14th International Symposium on Turbulence and Shear Flow Phenomena (TSFP14)
Heidelberg, Germany, July 28–31, 2026

A BROAD DOWNSTREAM-REGION PIV MEASUREMENT AND MODE ANALYSIS OF COUETTE AND POISEUILLE FLOWS OVER A FORWARD FACING STEP

Toru Yamada
Graduate School of Engineering
Nagoya Institute of Technology
Gokiso-cho, Showa-ku, Nagoya, Japan
email: yamada.toru@nitech.ac.jp

Ryuichi Tanaka
Graduate School of Engineering
Nagoya Institute of Technology
Gokiso-cho, Showa-ku, Nagoya, Japan
email: r.tanaka.250@stn.nitech.ac.jp

Yusuke Okochi
Graduate School of Engineering
Nagoya Institute of Technology
Gokiso-cho, Showa-ku, Nagoya, Japan
email: y.okochi.891@stn.nitech.ac.jp

Yohei Morinishi
Graduate School of Engineering
Nagoya Institute of Technology
Gokiso-cho, Showa-ku, Nagoya, Japan
email: morinishi.yohei@nitech.ac.jp

ABSTRACT

This study experimentally investigates the flow structures of Couette- and Poiseuille-type turbulent channel flows downstream of a forward-facing step with a contraction ratio of 0.5 at Reynolds number 3000. Instantaneous velocity fields are measured using particle image velocimetry (PIV) with a high-speed camera over confined and broad downstream regions. The reliability of the broad-field measurements is validated by comparison with confined-region data. Proper orthogonal decomposition (POD) is applied to the high-speed PIV data to extract dominant spatial modes. The results reveal distinct differences in the downstream vortical structures between the two flow types, particularly in their wall-normal development. Spectral analysis of the modal coefficients further demonstrates differences in the dynamical characteristics of the two flows and highlights the importance of high temporal resolution in resolving the dominant flow behavior. Paired POD modes with comparable eigenvalues indicate that the Couette flow exhibits larger-scale vortices extending toward the moving wall, whereas the Poiseuille flow shows structures more confined near the upper wall. In addition, the broader frequency distribution of modal coefficients in the Poiseuille flow suggests more complex temporal dynamics than in the Couette flow.

INTRODUCTION

Flow over a forward-facing step (FFS) is characterized by two separation bubbles: one immediately downstream of the step, and another on top of the step. These bubbles play a crucial role in engineering performance metrics, such as pressure drop, heat-transfer efficiency, and aerodynamic drag, across applications, including wind-turbine blades, heat-exchanger cooling channels, and vehicle underbodies. For this reason, suppression of separation or optimization of the reattachment location is a key factor to enhance operational efficiency and reliability.

Previous studies on FFS flows include both experimental and numerical investigations, which have revealed the complex flow dynamics, for example, a wide range of frequency components involved in the flow (Kiya & Sasaki (1983)), statistically two dimensional flow structures in the spanwise direction for a wide width-to-height ratio (Sherry *et al.* (2010)), and inherently three-dimensional fluctuations (Largeau & Moriniere (2006)). Also, the formation and growth of the separation bubble are confirmed to depend on various parameters, including boundary layer thickness, turbulence level, step height, and Reynolds number (Sherry *et al.* (2010)). However, previous FFS studies seem to mainly focus on its effects in boundary-layer flows, while investigations in channel-flow configurations remain limited. In particular, studies treating the downstream flow purely as wall-driven shear (Couette) flow remain extremely limited. Our recent study (Yamada *et al.* (2022)) experimentally performed the parallel-plate channel flow over a FFS where purely Couette flow was treated in the downstream region, where the measurement was confined to a region close to the stationary wall and the flow field of a broader region including the moving wall while the far downstream areas is missing. It is, however, essential to capture the broad velocity field to clarify the comprehensive mechanisms governing the transport involving breakdown of vortices and the effect of the wall.

In this study, a set of experiments is conducted to investigate the flow structures of Couette and Poiseuille turbulent channel flows in a broad downstream region of a FFS having a contraction ratio of 0.5. The flows are captured with a high-speed (HS) camera, and the instantaneous velocity fields are measured by the Particle Image Velocimetry (PIV). We apply Proper orthogonal decomposition (POD) to the PIV data for both the flow types. The flow structures extracted by the POD are compared, and the difference of those in the broad downstream region is discussed.

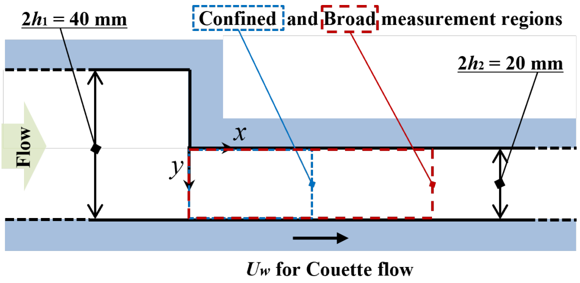

Figure 1. Schematic of the PIV measurement of the FFS flow in the present study.

EXPERIMENTAL METHODOLOGY

Experimental setup

Figure 1 illustrates the schematic of experiments in the present study. Air seeded with olive-oil mist enters the test section—a parallel-plate channel 865 mm wide—then encounters a sudden contraction at a forward-facing step located 3,500 mm downstream of the inlet before exiting the channel. By engaging or disengaging the lower moving wall, we produce either Couette or Poiseuille flow. In this study, the contraction ratio $\mathrm{CR} = h_2/h_1$, where h_1 and h_2 are the channel half-heights upstream and downstream of the step, respectively, is fixed at 0.5. The Reynolds number is set at 3,000 for both flow types, yielding the cases termed C3000 (Couette) and P3000 (Poiseuille). The Reynolds number for the Couette flow is defined as $Re = \frac{1}{2}U_w\,(2h_2)\,/\,\nu$, where U_w denotes the velocity of the moving wall and ν is the kinematic viscosity of air. For Poiseuille flow, $Re = U_{c_2}\,(2h_2)\,/\,\nu$, where U_{c_2} is the centerline velocity of the fully developed downstream flow. The flow was captured with an HS camera (Photoron Co., Ltd.) at 10 kHz with a spatial resolution of 1280 × 480 pixels. A continuous-wave laser (5 W, Kato Koken Co., Ltd.) was used to generate a laser sheet, and instantaneous velocity fields were measured via the PIV method. The experiments were performed for two velocity measurement frames, i.e., $0 < x/h_2 < 4$ (Broad) and $0 < x/h_2 < 2$ (Confined). The latter is performed to validate the accuracy of the measurement with the former measurement frame. For validation of statistical quantities, additional CCD-PIV measurements were performed at 5 Hz in the confined region only.

Proper orthogonal decomposition (POD)

The proper orthogonal decomposition (POD) technique leverages singular value decomposition (SVD) to decompose a data matrix into an ordered set of orthogonal modes, revealing the dominant structures in a dynamical system (Lumley (1989)). It has been widely applied in fluid dynamics to extract coherent structures from complex flow fields including FFS flows (Podvin & Fraigneau (2024)).

For the POD analysis in fluid dynamics, instantaneous snapshots $\mathbf{x}_1, \mathbf{x}_2, \ldots, \mathbf{x}_k$ are gathered into the matrix $\mathbf{X} = [\mathbf{x}_1, \mathbf{x}_2, \ldots, \mathbf{x}_k]$. Decomposing $\mathbf{X}$ via SVD yields $\mathbf{X} = U\Sigma V^*$, where * denotes the conjugate transpose. The spatial POD modes reside in the columns of U, while V encodes their temporal evolution. After computing Σ and V from the eigendecomposition of $\mathbf{XX}^*$, the modes in U can be recovered directly as $U = \mathbf{X}V\Sigma^{-1}$. For the purpose of reducing computational cost, the present study performed the Snapshot POD method (Sirovich (1987)), which computes the eigenvalues and eigenvectors of the smaller matrix $\mathbf{X}^*\mathbf{X}$, rather than the larger covariance matrix $\mathbf{XX}^*$, which results in the same spatial modes as the standard POD.

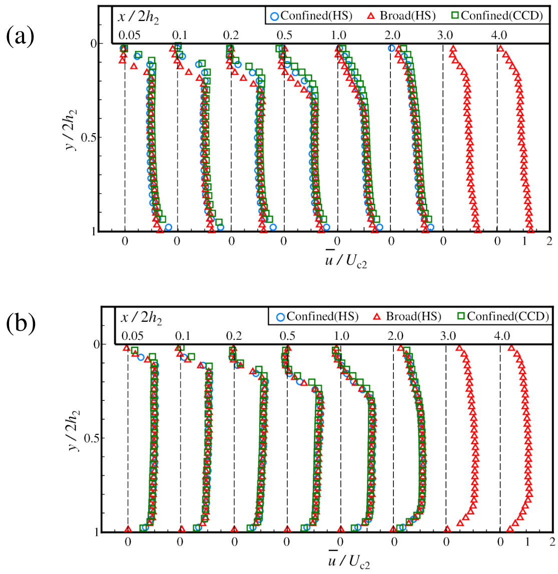

Figure 2. Streamwise mean velocity profiles for the (a) C3000 and (b) P3000 flows at different locations along the channel downstream for both Broad and Confined frames.

RESULTS AND DISCUSSION

The flow over a forward-facing step exhibits quasi-periodic behavior in the spanwise direction, characterized by the formation and evolution of separation bubbles. These bubbles, which appear downstream of the step, undergo cycles of growth and shrinkage with development and shedding of vortices. The key flow structures involved in this dynamic process can be effectively identified using POD analysis.

Mean velocity profile

Figure 2 shows the average streamwise velocity profiles for the Couette (Fig. 2(a)) and Poiseuille (Fig. 2(b)) flow types at different locations along the downstream of the channel for both Broad and Confined frames measured using the HS camera and CCD camera (only for the Confined frame). It is observed from the figure that there is an adverse-flow region near the upper (stationary) wall for both the flows up to approximately $x/2h_2 = 1.0$. First, comparing the velocity profiles between the HS and CCD measurements for the Confined frame, they are in good agreement with each other in both qualitative and quantitative manners while some minor discrepancies are present around the adverse-flow region for C3000. This agreement between the two different measurement techniques validates the accuracy of the velocity field obtained by the HS camera, which is used for the measurement of the Broad frame. Next, the comparisons of the velocity profiles between the Broad and Confined frames obtained by the HS camera, it is observed that they are in good agreement with each other in both qualitative and quantitative manners up to $x/h_2 = 2.0$ for both flow types, indicating that the frame size does not significantly influence the mean velocity field within this region. Comparing the flow profiles near the lower (moving) wall between the Couette and Poiseuille flow types, the flow for the former type exhibits a rise in velocity toward the wall due to the wall's motion, and vice versa for the latter case, which is consistent with the fundamental characteristics of each flow type. Furthermore, when focusing on the profiles for $x/h_2 \geq 3$, it can be confirmed that the profile becomes stable for both flow types, indicating that the region strongly influenced by the separation bubble is within $x/h_2 < 3$.

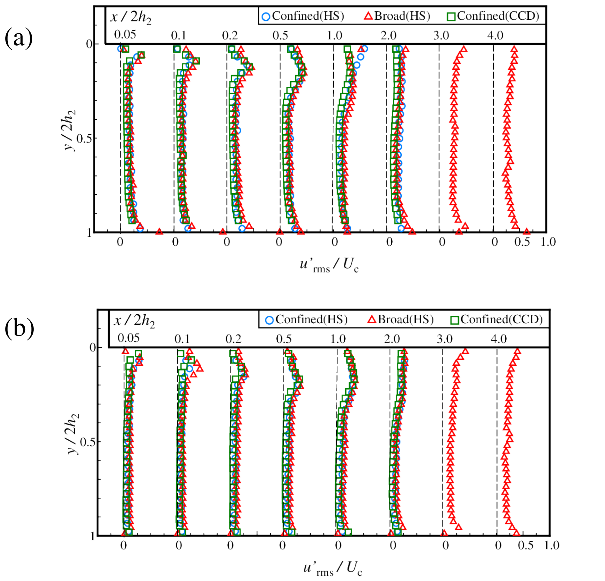

Figure 3. Streamwise turbulence intensity profiles for the (a) C3000 and (b) P3000 flows at different locations along the channel downstream for both Broad and Confined frames.

Turbulence intensity profile

Figure 3 shows the turbulence intensity profiles for the Couette (Fig. 3(a)) and Poiseuille (Fig. 3(b)) flow types at different locations along the downstream of the channel for both the Broad and Confined frames. It is observed from the figure that, for both flow types, turbulence intensity reaches high levels and exhibits abrupt changes near the upper wall. This region is identical to that where the adverse-flow occurs as shown in Fig. 2, indicating that this strong turbulence is produced by the large velocity gradient at the interface between the separation bubble and the main flow. First, comparing the turbulence intensity profiles between the HS and CCD measurements for the Confined frame, they are in good agreement with each other in both qualitative and quantitative manners, which is the same observation as in Fig. 2 and thus validates the accuracy of the velocity field obtained by the HS camera at least for the Confined frame. Comparing the profiles between the Broad and Confined frames for the HS camera up to $x/h_2 = 2.0$, the discrepancy is the same level as that for the mean velocity shown in Fig. 2. Focusing on the profiles for $x/h_2 \geq 3.0$, it is observed that the turbulence intensity increases and does not approach zero in the vicinity of the upper wall for both flow types. This is probably due to the experimental conditions, such as the spatial resolution, duration of the data acquisition, and time interval between the images for PIV measurement.

POD analysis

First, the POD modes obtained from the Confined and Broad frames are compared. Figure 4 shows the Mode 1 extracted from the Confined frame (Fig. 4(a)) and the Broad frame (Fig. 4(b)) for the C3000 flow. The figure demonstrates, in the Broad frame, that the region with dark blue contour along the top wall is extended into far downstream of the FFS ($x/2h_2 \approx 4.0$) and it spreads over the half channel width ($y/2h_2 = 0.5$). Whereas, the whole structure cannot be observed from Mode 1 from the Confined frame. The same observation is provided from Fig. 5 for the P3000 flow. Comparison between Figs. 4(a) and 5(a) of the Confined frames seemingly provides an insight that these structures are similar to each other. However, in that between the Broad frames,

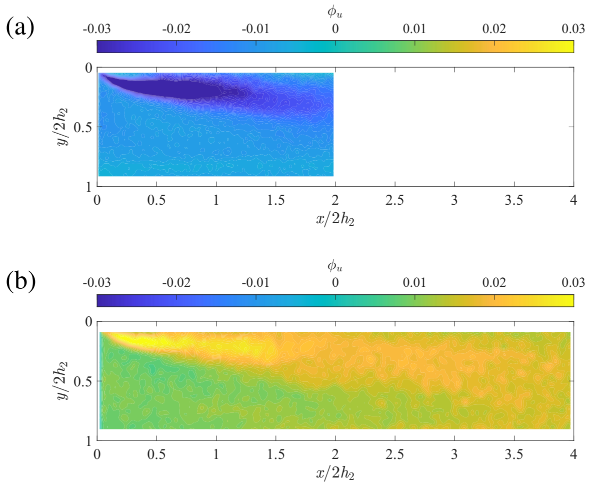

Figure 4. Mode 1 extracted from the (a) Confined and (b) Broad frames for C3000.

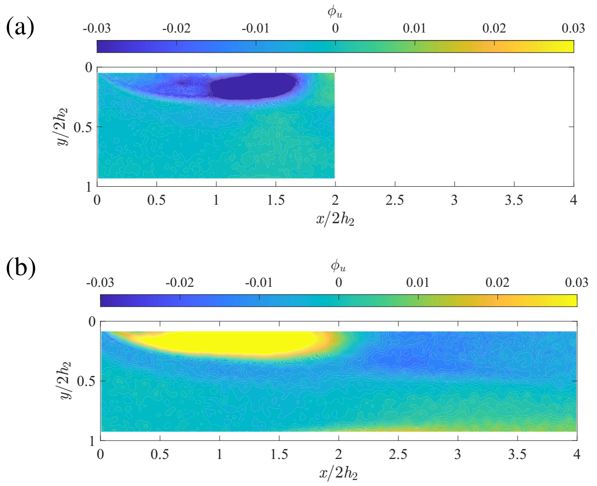

Figure 5. Mode 1 extracted from the (a) Confined and (b) Broad frames for P3000.

Fig. 5(b) shows the characteristic structures for the P3000 flow can be observed only in the upper half of the channel, whereas these for the C3000 flow are extended into that region. This difference is considered due to the existence of the lower-wall's motion.

Figure 6 shows the normalized eigenvalue spectra of the POD modes for the C3000 and P3000 flows obtained from the Broad-frame data. In both cases, Mode 1 has a prominently larger eigenvalue than the subsequent modes, indicating that the structures shown in Figs. 4 and 5 dominate the downstream region of the FFS. On the other hand, a clear paired mode with an eigenvalue comparable to that of Mode 1 is not observed. Therefore, the dynamical behavior associated with Mode 1, and the differences between the two flow types, cannot be directly discussed from the present POD results.

To compare the dynamical behavior between the C3000 and P3000 flows, we instead focus on clear pairs of modes with comparable eigenvalues, which is a common approach in POD analysis. As seen in Fig. 6, Modes 4 and 5 form such a pair for the C3000 flow, whereas Modes 2 and 3 form a pair for the P3000 flow. The dynamical behaviors of these paired modes are compared in the following paragraphs.

The level of agreement between the paired modes, in both their spatial structures and temporal behavior, is examined sep-

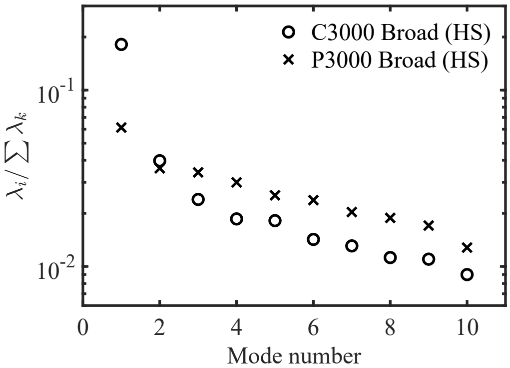

Figure 6. Ratio of eigenvalues for the POD modes for the C3000 and P3000.

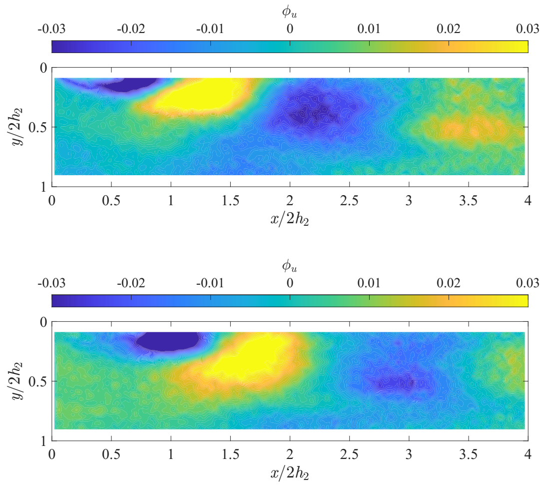

Figure 7. POD (a) Mode 4 and (b) Mode 5 extracted from the C3000 flow.

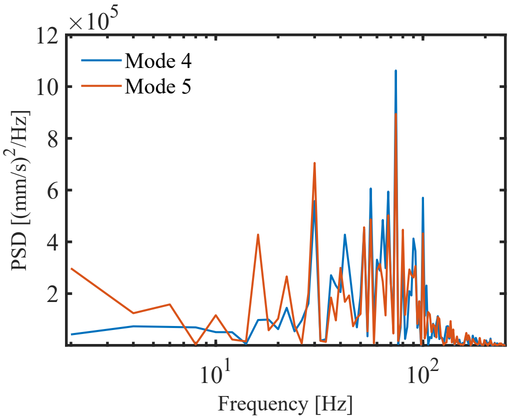

Figure 8. Power spectral density of the POD coefficients for Mode 4 and Mode 5 of the C3000 flow.

arately for the C3000 and P3000 flows. Figure 7 shows the spatial structures of Mode 4 and Mode 5 for the C3000 flow. As can be seen from the figure, both modes exhibit similar structures, characterized by an alternating pattern of positive (red) and negative (blue) regions along the streamwise direction whose size gradually increases and almost reaches the upper wall in the downstream region. The reconstructed flow fields using these modes (not shown here) also show that the vortices ejected from the separation bubble grow in size and

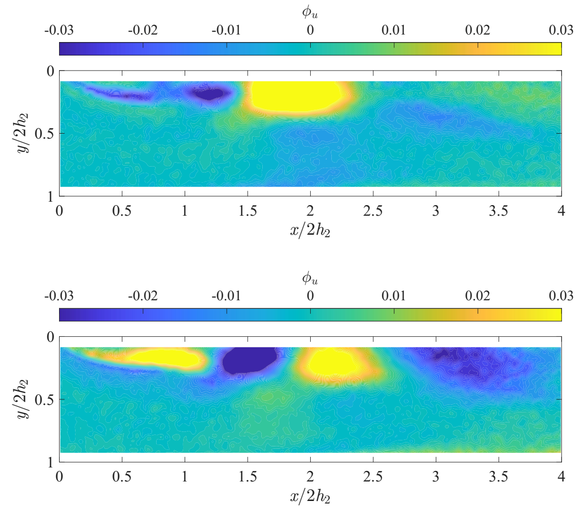

Figure 9. POD (a) Mode 2 and (b) Mode 3 extracted from the P3000 flow.

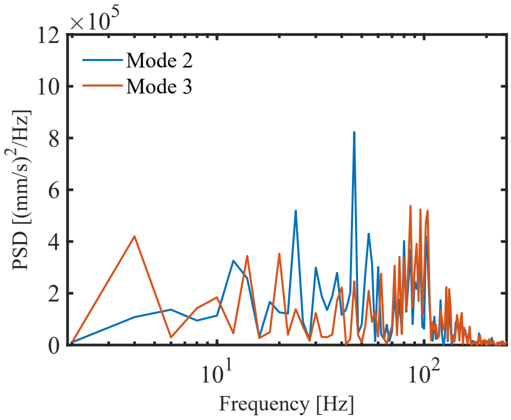

Figure 10. Power spectral density of the POD coefficients for Mode 2 and Mode 3 of the P3000 flow.

reach the lower wall in the downstream region. Figure 8 shows the power spectral density (PSD) of the POD coefficients for these modes, demonstrating that the dominant frequencies for both modes approximately correspond to each other. Therefore, these modes can be considered as a pair representing a single dynamical behavior.

Figure 9 shows the spatial structures of Mode 2 and Mode 3 for the P3000 flow. This figure shows good correspondence between the two modes while partial discrepancies are observed in the downstream region. The movie of the reconstructed flow using these modes (will be shown in the presentation) suggests that the vortex motion in P3000 is less smooth than that in the C3000 flow, exhibiting a more intermittent and less coherent evolution. Also, the agreement of the PSD of the POD coefficients for these modes, shown in Fig. 10, is not as good as that for the C3000 flow, indicating that these modes are less coherent as those for the C3000 flow. It is likely that the POD does not isolate the targeted structure in the P3000 flow as clearly as in the C3000 flow, so that the expected coherent structure is partially spread across multiple modes.

Comparing the flow fields using the paired modes between the C3000 and P3000 flows, it is obvious that the extracted structures for the C3000 flow (Fig 7) involve larger-scale vortices that reach the lower (moving) wall than those for the P3000 flow moving along the upper (stationary) wall

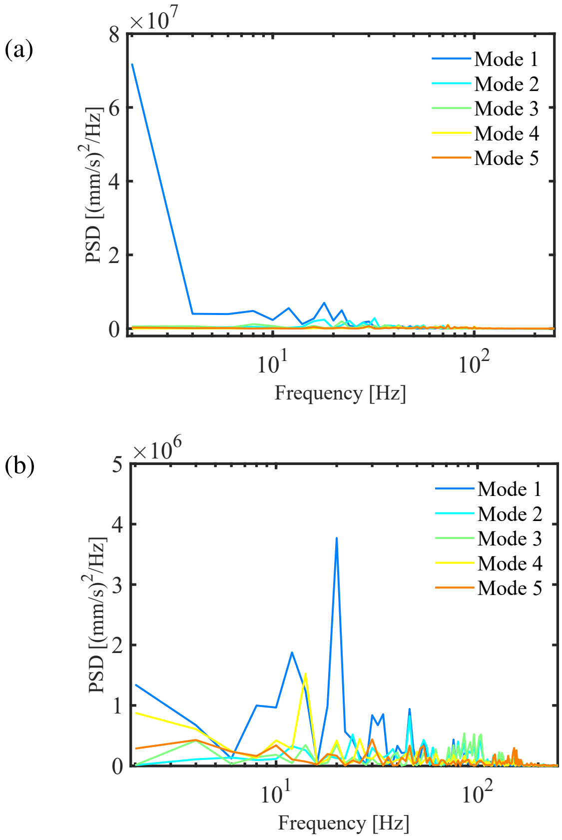

Figure 11. Power spectral density of the POD coefficients of the POD modes from Mode 1 to Mode 5 for the (a) C3000 and (b) P3000 flows.

(Fig 9). This is considered to be due to the difference in the total shear stress profiles between the two flow types: That for the C3000 flow is uniform along the wall-normal direction, whereas that for the P3000 flow has a zero value at the channel center and a maximum value at the walls. This difference leads to the difference in the energy supply mechanism for the growth of the vortices. The vortices shedded from the separation bubble for the P3000 flow cannot grow in size due to the smaller velocity gradient at the center of the channel preventing the energy supply from the mean flow. On the other hand, for the C3000 flow, the vortices can constantly grow in size by extracting energy from the mean flow resulting from the uniform shear stress profile. As not presented in this paper, the POD modes for the higher modes also show the same trend. This difference in the growth of the vortices is considered to be one of the key factors influencing the difference in the flow characteristics in the downstream region of the FFS between the Couette and Poiseuille flow types.

Finally, the difference in the temporal behavior of the flow structures between C3000 and P3000 flows is compared by the PSD of the POD coefficients. Figure 11 shows the PSD of the POD coefficients of the POD modes from Mode 1 to Mode 5 for the C3000 (Fig. 11(a)) and P3000 (Fig. 11(b)) flows. As can be seen from the figure, for the C3000 flow, the PSD for Mode 1 is prominently larger than those of the higher modes, and its dominant frequency is 2 Hz while other peaks are also observed at larger frequencies smaller than 50 Hz. The PSD for the higher modes also shows some peaks although they are almost negligibly small compared to that for Mode 1. On the other hand, for the P3000 flow, although the PSD for Mode 1 is also the dominant one as in the C3000 flow, those for the higher modes are relatively large indicating that these modes are involved in the flow dynamics more significantly than those for C3000 flow. Also, the peaks for the P3000 flow are observed at a wider range of frequencies than those for the C3000 flow. This indicates that the flow dynamics for the P3000 flow is more complex than that for the C3000 flow, which will be further investigated in the future work.

CONCLUSIONS

This study presents a comprehensive experimental investigation of the flow structures in Couette and Poiseuille turbulent channel flows downstream of a forward-facing step at Reynolds number 3000 using PIV measurements and POD analysis. The key findings are as follows: (1) By extending the measurement region to a broader downstream area, the flow structures extracted by the POD revealed distinct differences between the two flow types that were not fully captured in the confined measurement region. (2) The paired POD modes were chosen in terms of their eigenvalues, and the key differences in spatial structures between the two flow types were observed, i.e., the Couette flow exhibited larger-scale vortices that reached the lower wall, while the Poiseuille flow showed smaller vortices along the upper wall. These differences can be attributed to the difference in the shear stress profiles of the two flow types where the energy supply mechanism for the growth of the vortices is different. (3) Temporal behavior of the flow structures was analyzed by the power spectral density of the POD coefficients. The results showed that the temporal dynamics of the flow structures differ significantly between the two flow types, with the C3000 flow exhibiting frequency peaks at a smaller range of frequencies than the P3000 flow, indicating that the flow dynamics for the P3000 flow is more complex than that for the C3000 flow.

This work was supported by JSPS KAKENHI Grant Number JP25K07583.

REFERENCES

Kiya, M. & Sasaki, K. 1983 Structure of a turbulent separation bubble. *Journal of Fluid Mechanics* **137** (-1), 83–113.

Largeau, J. F. & Moriniere, V. 2006 Wall pressure fluctuations and topology in separated flows over a forward-facing step. *Experiments in Fluids* **42** (1), 21–40.

Lumley, J. L. 1989 The state of turbulence research. In *Advances in Turbulence* (ed. Roger Arndt William K. George). Hemisphere Pub. Co.

Podvin, B. & Fraigneau, Y. 2024 Low-dimensional analysis and modelling of the flow over a forward-facing step. *Journal of Fluid Mechanics* **1000**, A69–1–A69–36.

Sherry, M., Lo Jacono, D. & Sheridan, J. 2010 An experimental investigation of the recirculation zone formed downstream of a forward facing step. *Journal of Wind Engineering and Industrial Aerodynamics* **98** (12), 888–894.

Sirovich, L. 1987 Turbulence and the dynamics of coherent structures part I: Coherent structures. *Quarterly of Applied Mathematics* **45** (3), 561–571.

Yamada, T., Sugisaka, T., Tamano, S. & Morinishi, Y. 2022 POD and DMD mode analyses of Poiseuille and Couette flows over 1/2-contraction-ratio forward-facing step. In *12th International Symposium on Turbulence and Shear Flow Phenomena, TSFP-12, 6* pages.